

Plastic flow and failure resistance of metallic glass: Insight from *in situ* compression of nanopillars

Z. W. Shan,^{1,4,*} J. Li,² Y. Q. Cheng,³ A. M. Minor,⁴ S. A. Syed Asif,¹ O. L. Warren,¹ and E. Ma^{3,†}

¹Hysitron, Inc., Minneapolis, Minnesota 55344, USA

²Department of Materials Science and Engineering, University of Pennsylvania, Philadelphia, Pennsylvania 19104, USA

³Johns Hopkins University, Baltimore, Maryland 21218, USA

⁴National Center for Electron Microscopy, Lawrence Berkeley National Laboratory, Berkeley, California 94720, USA

(Received 16 March 2008; published 14 April 2008)

We report *in situ* nanocompression tests of Cu-Zr-Al metallic glass (MG) pillars in a transmission electron microscope. This technique is capable of spatially and temporally resolving the plastic flow in MGs. The observations reveal the intrinsic ability of fully glassy MGs to sustain large plastic strains, which would otherwise be preempted by catastrophic instability in macroscopic samples and conventional tests. The high ductility in volume-limited MGs and the sample size effects in suppressing the rapid failure common to MGs are analyzed by modeling the evolution of the collectivity of flow defects toward localization.

DOI: [10.1103/PhysRevB.77.155419](https://doi.org/10.1103/PhysRevB.77.155419)

PACS number(s): 62.25.-g, 61.43.Dq, 62.20.F-, 68.37.Lp

I. INTRODUCTION

The metals and alloys in use today are all crystalline. In recent years, a number of novel amorphous alloys, called bulk metallic glasses (BMGs), have emerged as promising engineering materials. These BMGs possess many impressive properties such as superb strength and elastic properties, excellent formability in the supercooled liquid region, and high wear and corrosion resistance.¹ However, the BMGs have an Achilles' heel: they show little ductility at room temperature and are believed to be quasibrittle materials.^{1,2}

Crystalline metals are ductile because the long-range coherency in their structure allows the presence and movement of dislocations. These flow defects are the main carriers of plasticity. In an amorphous metal, entities that serve the functions of "flow defects" can be generated under stresses as well. This is because, although there are no obvious pre-existing flow defects to speak of in glass, inherent in the internal structure, there are structural and dynamical heterogeneities, i.e., local regions that have the ability to preferentially undergo "shear transformations" (STs) upon loading.³ In fact, these "shear transformation zones" (STZs) are believed to be small (containing ~ 100 atoms), numerous, and everywhere throughout the metallic glass (MG) body.^{2,3} Yet, MGs are not macroscopically ductile. Apparently, the STZs behave very differently from the dislocations in their crystalline counterparts. One obvious difference is that while dislocations interact and multiply to cause strain hardening that stabilizes plastic flow,⁴ the STs lead to dilatation (generation of free volume⁵) in their wake, causing a high collectivity of flow defects (STZs) and autocatalytic flow softening.⁶ In experiments, one observes a strong tendency for severe instability that sets in often at the very beginning of plastic deformation. The strains are highly inhomogeneous, exclusively localized in extremely narrow shear bands, which are 10–20 nm in thickness.^{2,7–14} Such shear banding can quickly lead to cracking and failure, rendering MGs macroscopically brittle. As a result, in numerous conventional tests that so far use millimeter-diameter samples, one observes virtually no homogeneous deformation.^{2,7–14} The

rapid shear banding process leaves no time for the actions of the STs, which could otherwise pop out all over the test sample, and also makes it difficult to experimentally resolve the strain evolution in space and time.²

In the following, we examine the plastic flow in small-volume (submicron-sized) MG samples. This is motivated by the expectation that with the limited deformation volume, the shear banding may be slow and less violent, and catastrophic localization could be suppressed to allow the observation of large contributions to uniformly spread out strains from STZs (see discussion below). Hints for changes in MG deformation modes have emerged recently,^{15–19} but the details and mechanisms are only beginning to be revealed.

A quantitative nanocompression test inside a transmission electron microscope (TEM) will be employed, which will monitor *in situ* the evolution of the plastic flow in MG pillars. This approach has obvious advantages. First, it allows us to watch the deformation as it happens, correlating the measured force-displacement response (such as pop-in) at $\sim 0.3 \mu\text{N}$ and $< 1 \text{ nm}$ resolutions with time-resolved TEM images (movie).²⁰ Second, one observes the exact sample geometry and punch location, which is important for interpreting the test data. Third, electron diffraction patterns and dark-field imaging directly reveal whether nanocrystallization occurs during deformation;^{21,22} *in situ* structural information is crucial for understanding the deformation micro-mechanisms.

II. EXPERIMENTS

Five monolithic $\text{Cu}_{46}\text{Zr}_{47}\text{Al}_7$ MG samples with dimensions of a few hundreds of nanometers have been studied. The material was prepared using melt spinning. Bulk (millimeter-sized) metallic glass can also be made at this alloy composition, which showed a yield strength of $\sim 2000 \text{ MPa}$ and a compressive plastic strain of $< 1\%$ before failure.²³ Cylindrical nanopillars for our *in situ* compression experiments were made by employing the focused ion beam (FIB) micromachining technique with a very low current (10 nA).²⁴ *In situ* nanocompression experiments were carried

out at room temperature in a JEOL 3010 TEM operating at 300 kV, using a Hysitron TEM PicoIndenter that employs a miniature actuatable capacitive transducer equipped with a flat diamond punch, which generates load and measures the resultant vertical displacement, and a piezoelectric actuator for fine scale positioning of the transducer and/or punch relative to the pillar. Two samples with similar physical dimensions, i.e., ~ 330 nm in diameter at the bottom (fixed end), 410 nm in height and 10° in side wall taper, will be described in detail below, as they displayed representative behavior for the samples tested. Their diameters are much larger compared to the penetration depth (~ 10 nm) of the Ga ions used in the FIB cutting. The two amorphous samples, hereafter referred to as sample I and sample II, were compressed under an open-loop load control ($14 \mu\text{N/s}$ for 10 s of increasing load) and displacement control (10 nm/s for 10 s of increasing displacement), respectively. The tests were recorded via videotaping at a rate of 30 frames/s in the microscope. Beam-heating effects are considered to be minimal since our pillar specimen was part of a much larger MG piece in contact with a flat diamond punch of high thermal conductivity that is very large relative to the pillar.

III. RESULTS

Figures 1(a)–1(f) are representative dark-field TEM images of sample I, which were taken from the video recordings during a load-controlled nanocompression test.²⁵ Due to the taper from FIB cutting of such nanosized pillars, the plastic deformation was confined to start from the top (contact interface with the punch) of the pillar. The top half of the pillar flowed to very large strains, $\sim 40\%$ in length changes [compare Fig. 1(a) with Fig. 1(f)]. Note from Fig. 1 and Ref. 25 that throughout the deformation, there was no apparent crystallization, and the deformation was not all localized on a single shear plane. The V-shaped “notches” on both sides of the pillar in Fig. 1(f) were not shear offsets due to shear banding (not the right direction and angle). As is clear from Ref. 25, they were formed when the top part was pushed to flow outward, overflowing past the bottom half of the pillar that did not deform much due to the taper.

Apparently, due to the confinement of both the sample size and geometry (taper and the resulting constraint), the catastrophic shear banding we are familiar with in conventional compression tests of normal sized MG samples did not occur. However, from the corresponding load-displacement curve shown in Fig. 2, we still see a number of displacement bursts, the largest of which was ~ 15 nm. In macroscopic samples, such displacement bursts in load-controlled tests (or load drops in displacement-controlled tests) are associated with sharp, planar shear bands with micrometer-sized shear offsets.²⁶ However, in our nanopillar (Fig. 1 and Ref. 25), these shear events are small and spread out. The strain did not spatially concentrate in an obvious, large shear band. Postdeformation TEM and scanning electron microscopy observations of the sample profile also confirmed that there was no major shear offset. Apparently, the many displacement bursts corresponded to multiple shear events that did not localize severely. Each displacement burst in Fig. 2, how-

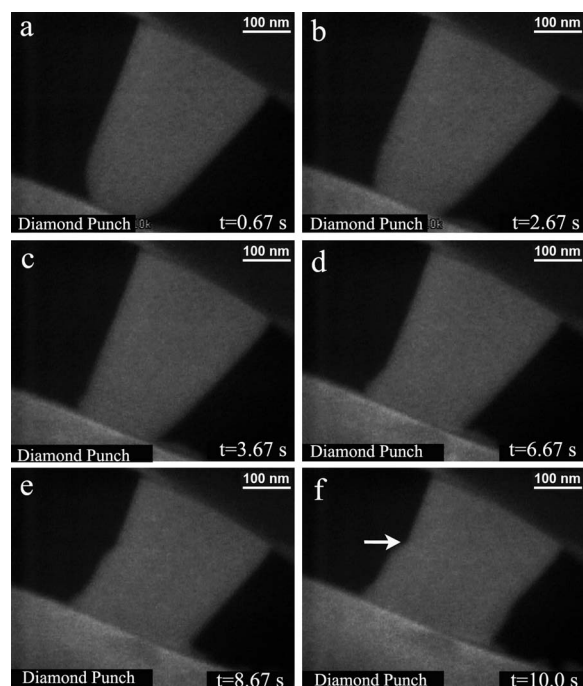


FIG. 1. *In situ* dark-field TEM observation of the compression of a metallic glass pillar. The different stages of the nanocompression process are depicted by individual still frames [(a)–(f)] at different times ($t=0$ s at the beginning of the test), extracted from a dynamic video sequence. Due to the taper geometry, the plastic deformation was gradually driven down from the top (contact interface) of the pillar, while the bottom part remains largely elastic. No major shear was observed until the end of the programmed compression displacement. The notch marked by the white arrow in Fig. 1(f) is not a shear offset (see text). Near the end of the test, a faint line of contrast appeared from the notch (more visible in the movie), suggesting that a major shear eventually set in from this stress concentrator. The entire continuous flow process is documented in Ref. 25.

ever, may already be due to a group of STZs and more than one local unit shear event. Temporally correlated but not obviously spatially correlated shear relaxation events had been previously observed in earthquakes and granular media.²⁷ The discrete shear events in the amorphous pillars here are small, and a large number of them are closely spaced in a small volume over a total displacement distance of only ~ 100 nm. This renders the plastic flow to appear nearly “homogeneous”.^{15,16,19} The plastic deformation is homogeneous in the sense that, much like in crystalline metals, flow carriers are active everywhere even though they themselves are discrete.

The same behavior was repeatedly captured to various extents in our five samples. For example, sample II in Fig. 3 in a displacement-controlled experiment experienced obvious shortening accompanied by an increase in diameter. In this case, however, a major shear did set in concurrently. Here, the pillar was pressed briefly once, and the load was removed. Upon reloading, a “shear band” was initiated. This relatively large shear cut across the entire sample, causing a shear step on the side (marked by an arrow). A movie showing the progression of this shear step is given in Ref. 25.

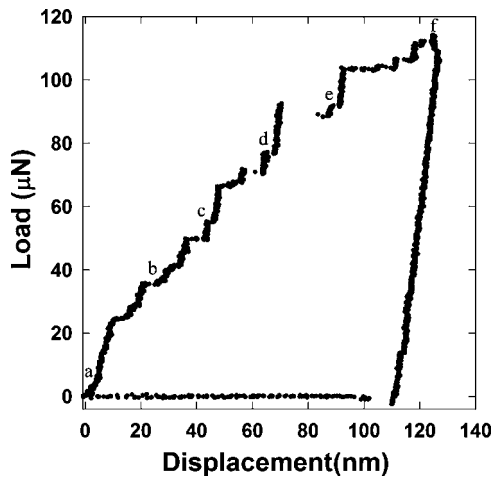


FIG. 2. Load vs displacement curve that corresponds to the load-controlled compression test. The various stages corresponding to those shown in Fig. 1(a)–1(f) are marked with letters. Note that displacement bursts are frequently observed with the largest one up to 15 nm.

With continued loading, a major portion of the subsequent deformation occurred in this same location, as seen in Figs. 3(b)–3(e). However, the reduction in sample height and increase in lateral dimensions cannot be fully accounted for from the strain due to the shear offset alone. In other words, there appears to be a homogeneous flow in the sample in addition to the advance of the offset itself.

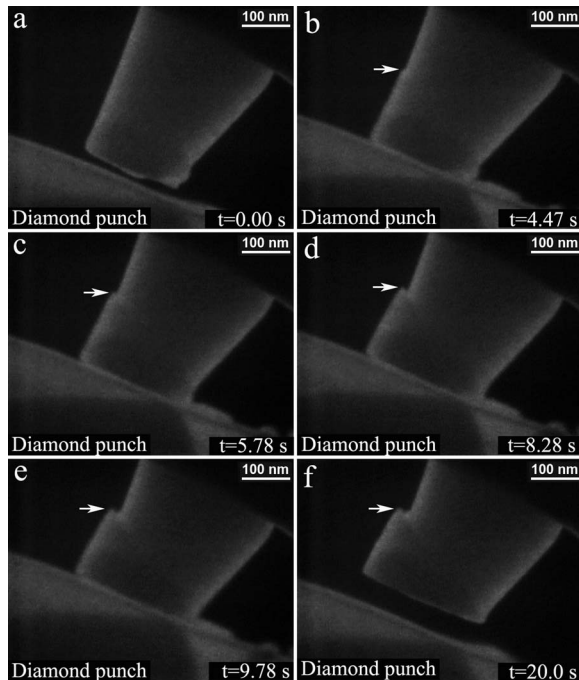


FIG. 3. *In situ* dark-field TEM observation of the formation and evolution of a major shear. The individual still frames [(a)–(f)] are extracted from a dynamic video sequence. The growing shear offset is indicated by the white arrow shown in (b)–(f) (see video in Ref. 25 for the jerky advancement of the shear offset and the flow of the MG outside the shear band region).

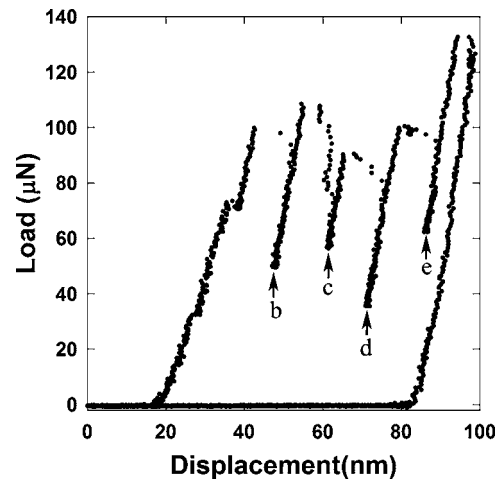


FIG. 4. Load vs displacement curve for the displacement-controlled compression test. The various stages corresponding to those shown in Fig. 3(b)–3(e) are marked with letters. The load drops in the curve are observed to synchronize with the jerky advancement of the shear step seen during the compression test (see Ref. 25).

The shear offset growth proceeded slowly, even when the total nominal plastic strain for the sample reached $\sim 21\%$, without the rapid shear rupture and fracture as in macroscopic MG samples.¹⁰ The sample absorbed much plastic work, including repeated shear events bursting in the same band. Serrations were obvious in the load-displacement curve in Fig. 4 and the load drops in the curve synchronized very well, in a one-to-one correspondence, with the jerky advancement of the shear step seen in Ref. 25. A close inspection reveals that the shear displacement rate in each jerky motion was only a small fraction of $1 \mu\text{m/s}$, releasing energy in a stepped and controlled fashion, which is different from macroscopic samples. In the latter case, the shear displacement avalanche driven by the large accumulated energy runs like a crack, at a rate of $>100 \mu\text{m/s}$, up to the speed of sound,^{2,28} orders of magnitude above the speed required for following the imposed nominal strain rate (typically $<10^{-3}/\text{s}$). Also different there is the fact that the serrations^{11–14} come from consecutive, multiple shear bands at different locations.

Note that in all of the five samples we tested, there was no rupture or fracture. There was also no apparent change of contrast due to crystallization throughout the *in situ* TEM dark-field observation, even in the offset regions near the edges of the cylindrical sample, which are very thin and heavily deformed. This is also supported by inspecting the diffraction patterns and postdeformation still images (not shown). Bright nanometer-scale crystals were seen in the dark-field images only when the diamond punch was repeatedly tapping the asperities on the contact surface, presumably causing friction and local heating. Therefore, the large plasticity observed here comes entirely from the flow of the monolithic glass, which is very different from the deflection and branching of shear bands due to nanocrystals, as suggested previously for some MGs,^{10,12,29} and from the microcracking of brittle materials. It is also different from the ho-

mogeneous deformation at elevated test temperatures⁵ near the glass transition temperature (~ 700 K for our MG), where large ductility is achieved through viscous flow.³⁰ The low deformation temperature in our tests is not only supported by the serrated flow and the lack of crystallization, but also by the estimate that the strength of the glass pillar is higher than those reported for macroscopic samples (the strength is expected to be lower if the sample temperature is significantly elevated due to beam heating).

IV. DISCUSSION

There appears to be remarkable sample size effects in the plastic flow and failure resistance of MGs. In the following, we present a simple model to explain why catastrophic strain localization and rupture are suppressed. Additional discussions on other perspectives for this issue can be found elsewhere.^{15–19}

Shear localization in MG is a collective phenomenon of flow defects, the smallest of which are the individual STZs $\sim 1 \text{ nm}^3$ in size.^{2,3,18,31} At low temperatures under constant stress, the STZs initially operate stochastically independent of each other, but they gradually gain correlation both temporally and spatially, and self-organize into a larger and larger flow zone.^{31,32} Such growth may proceed as a scale-free network^{33–36} with distinct spatial and temporal correlation patterns³⁷ that change with time, such that greater and greater percentages of the total strain are localized in the few most collective flow defects, approaching the final catastrophe that may involve significant thermal softening as well.³⁸ All these happen quickly in uniformly loaded macroscopic samples, since the total amount of stored elastic energy that feeds the growth into a runaway shear band is tremendous. With decreasing sample volume, this total energy decreases faster than the area associated with the localized shear,¹⁹ such that in our nanopillars the growth in collectivity may be arrested at an early stage. We are monitoring the birth and evolution of the primordial collective flow defect (larger than one STZ). Such an embryonic or incipient shear band is still much less collective, much slower, and much cooler in temperature than the final, mature shear band that emerges out of a macroscopic sample and is capable of destroying it. As such, the primordial STs in the deforming volume give rise to large strains that are either seemingly homogeneous (akin to dislocation plasticity in crystals, although the flow in MG cannot be attributed to “dislocations”), or at least stable (unlike a crack) if inhomogeneous. Nanocrystallization,^{10,21,22,29} which we did not observe, is more likely to occur in larger, faster, and hotter shear bands that appear in the later stages of shear band evolution.

By making a drastic simplification of the above dynamics, a scaling relation can be derived between the sample size L , and the useful plastic strain (tensile or compressive) ε_p , in the sample before failure. Let us consider a contiguous MG volume $\Omega=L^3$, consisting of N volume elements,

$$N = \Omega/\Omega_0 = (L/L_0)^3, \quad (1)$$

where $\Omega_0=L_0^3$ is the size of one potential STZ. For simplicity, assume that the collectivity of flow defects undergoes a

sharp step transition, from completely uncorrelated STZ “ideal gas” to completely correlated catastrophic localization (failure), when the uncorrelated STZs by chance form a shear band embryo of critical size, assumed to be a planar disk of $n \times n \times 1=A$ spatially contiguous transformed STZs, where n is the number of STZs linked together in one direction. Let us assume the transformation of each STZ carries a plastic strain ~ 1 .¹⁸ So in the “completely uncorrelated” stage, the probability that any particular volume element has transformed is ε_p when the sample-averaged plastic strain is ε_p . As such, the probability of forming a critical embryo centered at a particular volume element is just ε_p^A . However, there are N possible centers in the sample, so the total probability of a critical embryo appearing anywhere in the sample may be well approximated by $N\varepsilon_p^A$, if ε_p is small. The sharp transition from uncorrelated to correlated flow that leads to subsequent failure occurs when $N\varepsilon_p^A$ reaches order 1. Therefore, before catastrophic localization intervenes, the homogeneous strain is of the order

$$\varepsilon_p \propto N^{-1/A} = (L/L_0)^{-3/A}. \quad (2)$$

This scaling law takes the form of a “Hall–Petch” relation, but is for the useful plastic strain rather than for the strength of the MG. Its origin is rather similar to the Weibull statistics,³⁹ which describe the reliability of brittle ceramics: a critical-sized defect anywhere in the sample will fail the entire sample, therefore small-volume samples are more failure resistant. The assumption leading to the relation above is admittedly too draconian: in reality, the collectivity of flow defects grows smoothly, instead of in a step-change fashion. It can also preferentially grow at already-existing weak locations with concentrated flow defects (or preexisting minor flaws such as those in Fig. 3). These details aside, an inverse scaling relation $\varepsilon_p \propto L^{-\alpha}$ is still likely.^{18,40} The exponent α may depend on the sample material and loading conditions.

V. CONCLUDING REMARKS

In summary, we have performed time- and spatially-resolved quantitative measurements to monitor the mechanical response of a metallic glass *in situ*. Plastic strains can be intrinsically large for monolithic MGs at low temperatures without brittle failure, provided that catastrophic instabilities are suppressed via confinements. One way to realize this is by limiting the deformation volume, which is the “real estate” available to develop runaway shear bands. Due to the sample size effects on the flow carrier and/or defect dynamics, there can be no shear band at all, or the shear bands formed are at least not as excessively energetic and threatening as in macroscopic samples. When mature, catastrophic shear bands leading to failure are suppressed, STs throughout the sample are given the opportunity to contribute to the overall plastic strain, leading to large (and sometimes apparently homogeneous) flow. We emphasize that the stable and gradual plastic flow observed here is carried by multiple organized STZ groups (including one that may be an embryonic shear band). In large samples, in contrast, shear bands are few and far between and their multiplication and/or deflection requires the presence of nanocrystals.

Aside from a fundamental understanding of the intrinsic behavior of amorphous metals in plastic deformation and fracture, the large plasticity and failure resistance in small-volume MGs can be exploited in designing components in microelectromechanical systems and nanoelectromechanical systems, thin films, and crystal-amorphous composites,^{16,18} for simultaneous high strength, ductility, and capacities for mechanical energy absorption. Our results also have implications for improving the plasticity of large MG samples. For example, during processing one can create an alloy with mixed crystals and metallic glass,^{11,12} multi-phase (phase-separated) MGs,^{41,42} or MG with considerable structural heterogeneities.⁴³ The material prepared as such would then contain small-volume compartments of very different properties. The contiguous MG volume of each compartment is made intentionally small and confined, such that when it undergoes plastic flow upon loading the growth of flow defect collectivity does not reach excessive levels. The localized shear could then be effectively blocked, deflected, or diffused by the interphase boundaries. Clearly, more systematic

experiments are needed to assess if there exists a critical size limit for the sample size effects on the ductility, fracture behavior, and strength of MGs. More modeling efforts are also needed, beyond the simple model presented here and the qualitative arguments in related publications.¹⁵⁻¹⁹

ACKNOWLEDGMENTS

The authors thank J. Wen and T.Z. Luo for assistance in sample preparation. J.L. acknowledges the support from NSF (DMR-0502711) and ONR (N00014-05-1-0504). A.M.M. was supported by the Scientific User Facilities Division of the Office of Basic Energy Sciences, U.S. Department of Energy under Contract No. DE-AC02-05CH11231. Y.Q.C. and E.M. were supported by the Division of Materials Science and Engineering, the Office of Basic Energy Sciences, U.S. Department of Energy under Contract No. DE-FG02-03ER46056. Z.W.S. and the instrument development were supported in part by a DOE SBIR Phase II grant (DE-FG02-04ER83979) awarded to Hysitron, Inc.

*zhiweishan@gmail.com

†ema@jhu.edu

¹A. L. Greer and E. Ma, MRS Bull. **32**, 611 (2007).

²C. A. Schuh, T. C. Hufnagel, and U. Ramamurty, Acta Mater. **55**, 4067 (2007).

³A. S. Argon and H. Y. Kuo, Mater. Sci. Eng. **39**, 101 (1979).

⁴E. Ma, Nat. Mater. **2**, 7 (2003).

⁵F. Spaepen, Acta Metall. **25**, 407 (1977).

⁶Q. Li and M. Li, Intermetallics **14**, 1005 (2006).

⁷C. A. Pampillo and H. S. Chen, Mater. Sci. Eng. **13**, 181 (1974).

⁸L. A. Davis and Y. T. Yeow, J. Mater. Sci. **15**, 230 (1980).

⁹J. J. Lewandowski and P. Lowhaphandu, Philos. Mag. A **82**, 3427 (2002).

¹⁰A. R. Yavari, J. J. Lewandowski, and J. Eckert, MRS Bull. **32**, 635 (2007).

¹¹C. C. Hays, C. P. Kim, and W. L. Johnson, Phys. Rev. Lett. **84**, 2901 (2000).

¹²A. Inoue, W. Zhang, T. Tsurui, A. R. Yavari, and A. L. Greer, Philos. Mag. Lett. **85**, 221 (2005).

¹³Z. F. Zhang, H. Zhang, X. F. Pan, J. Das, and J. Eckert, Philos. Mag. Lett. **85**, 513 (2005).

¹⁴H. Bei, S. Xie, and E. P. George, Phys. Rev. Lett. **96**, 105503 (2006).

¹⁵C. A. Volkert, N. Cordero, E. T. Lilleodden, A. Donohue, and F. Spaepen, in *Size Effects in the Deformation of Materials: Experiments and Modeling*, edited by E. Lilleodden, P. Besser, L. Levine, and A. Needleman MRS Symposia Proceedings No. 976E (Materials Research Society, Warrendale, PA, 2007), p. 0976-EE11-01.

¹⁶A. Donohue, F. Spaepen, R. G. Hoagland, and A. Misra, Appl. Phys. Lett. **91**, 241905 (2007).

¹⁷Q. Zheng, S. Cheng, J. H. Strader, E. Ma, and J. Xu, Scr. Mater. **56**, 161 (2007).

¹⁸Y. M. Wang, J. Li, A. V. Hamza, and T. W. Barbee, Proc. Natl. Acad. Sci. U.S.A. **104**, 11155 (2007).

¹⁹H. Guo, P. F. Yan, Y. B. Wang, Z. F. Zhang, J. Tan, M. L. Sui, and E. Ma, Nat. Mater. **6**, 735 (2007).

²⁰A. M. Minor, S. A. S. Asif, Z. W. Shan, E. A. Stach, E. Cyranowski, T. J. Wyrobek, and O. L. Warren, Nat. Mater. **5**, 697 (2006).

²¹H. Chen, Y. He, G. J. Shiflet, and S. J. Poon, Nature (London) **367**, 541 (1994).

²²J. J. Kim, Y. Choi, S. Suresh, and A. S. Argon, Science **295**, 654 (2002).

²³G. Kumar, T. Ohkubo, T. Mukai, and K. Hono, Scr. Mater. **57**, 173 (2007).

²⁴M. D. Uchic, D. M. Dimiduk, J. N. Florando, and W. D. Nix, Science **305**, 986 (2004).

²⁵See EPAPS Document No. E-PRBMDO-77-055815 for videotaped movies taken at 30 frames per second, for the *in situ* compression tests of the Cu₄₆Zr₄₇Al₇ metallic glass nanopillars in Figs. 1 and 3. For more information on EPAPS, see <http://www.aip.org/pubservs/epaps.html>.

²⁶W. H. Jiang, G. J. Fan, F. X. Liu, G. Y. Wang, H. Choo H, and P. K. Liaw, J. Mater. Res. **21**, 2164 (2006).

²⁷P. A. Johnson and X. P. Jia, Nature (London) **437**, 871 (2005).

²⁸Y. Zhang, W. H. Wang, and A. L. Greer, Nat. Mater. **5**, 857 (2006).

²⁹M. Chen, A. Inoue, W. Zhang, and T. Sakurai, Phys. Rev. Lett. **96**, 245502 (2006).

³⁰J. Lu, G. Ravichandran, and W. L. Johnson, Acta Mater. **51**, 3429 (2003).

³¹M. L. Falk and J. S. Langer, Phys. Rev. E **57**, 7192 (1998).

³²V. V. Bulatov and A. S. Argon, Modell. Simul. Mater. Sci. Eng. **2**, 203 (1994).

³³P. Hahner, K. Bay, and M. Zaiser, Phys. Rev. Lett. **81**, 2470 (1998).

³⁴M. C. Miguel, A. Vespignani, S. Zapperi, J. Weiss, and J. R. Grasso, Nature (London) **410**, 667 (2001).

³⁵D. M. Dimiduk, C. Woodward, R. LeSar, and M. D. Uchic,

- Science **312**, 1188 (2006).
- ³⁶A. L. Barabasi and R. Albert, Science **286**, 509 (1999).
- ³⁷W. H. Jiang, G. J. Fan, F. Liu, G. Y. Wang, H. Choo, and P. K. Liaw, Int. J. Plast. **24**, 1 (2008).
- ³⁸F. Shimizu, S. Ogata, and J. Li, Acta Mater. **54**, 4293 (2006).
- ³⁹Z. P. Bazant and S. D. Pang, J. Mech. Phys. Solids **55**, 91 (2007).
- ⁴⁰R. D. Conner, W. L. Johnson, N. E. Paton, and W. D. Nix, J. Appl. Phys. **94**, 904 (2003).
- ⁴¹Y. H. Liu, G. Wang, R. J. Wang, D. Q. Zhao, M. X. Pan, and W. H. Wang, Science **315**, 1385 (2007).
- ⁴²B. J. Park, H. J. Chang, D. H. Kim, W. T. Kim, K. Chattopadhyay, T. A. Abinandanan, and S. Bhattacharya, Phys. Rev. Lett. **96**, 245503 (2006).
- ⁴³J. Das, M. B. Tang, K. B. Kim, R. Theissmann, F. Baier, W. H. Wang, and J. Eckert, Phys. Rev. Lett. **94**, 205501 (2005).